Association-dissociation process with aging subunits: Recursive solution

Thomas Niedermayer* and Reinhard Lipowsky
Department of Theory and Bio-Systems, Max Planck Institute of Colloids and Interfaces, Am Mühlenberg 1, 14476 Potsdam, Germany
(Received 13 May 2015; revised manuscript received 31 August 2015; published 25 November 2015)

The coupling of stochastic growth and shrinkage of one-dimensional structures to random aging of the constituting subunits defines the simple association-dissociation-aging process which captures the essential features of the nonequilibrium assembly of cytoskeletal filaments. Because of correlations, previously employed mean-field methods fail to correctly describe filament growth. We study an alternative formulation of the full master equation of the stochastic process. An ansatz for the steady-state solution leads to a recursion relation which allows for the calculation of all emergent quantities with increasing accuracy and in excellent agreement with stochastic simulations.

DOI: 10.1103/PhysRevE.92.052137 PACS number(s): 05.40.−a, 82.20.−w, 87.10.Mn, 87.16.Ka

I. INTRODUCTION

A variety of dynamical phenomena, such as the assembly of cytoskeletal filaments [1], fibrillar aggregates [2], and synthetic supramolecular polymers [3], are stochastic growth and shrinkage processes of one-dimensional structures (filaments). Dynamical queues, which model telecommunication, computing, traffic engineering, and logistics processes, may also be described as randomly growing and shrinking filaments with calls, network packets, vehicles, or stock keeping units as respective subunits [4]. Transformations may change the subunit association and dissociation rates from the filament ends leading to altered filament growth and shrinkage rates.

In particular, irreversible transitions (aging) of the constituting subunits lead to characteristic assembly and disassembly cycles of cytoskeletal filaments [1,5]. Hydrolysis (aging) within actin filaments converts adenosine triphosphate (ATP) actin into adenosine diphosphate (ADP) actin [1]. Since ADP-actin has a larger dissociation rate than ATP-actin, the filaments become less stable as they grow older [1,6]. Similarly, the accelerated dissociation of tubulin caused by the hydrolysis of bound guanosine triphosphate (GTP) gives rise to the prominent dynamic instability of microtubules [1,7]. Moreover, the dynamics of various filaments of the bacterial cytoskeleton seem to be driven by a similar ATP(GTP) hydrolysis cycle [8]. While the precise modeling of cytoskeletal dynamics requires considerations of experimental details, such as the two-step ATP hydrolysis within actin filaments [1,9] or the protofilament interactions in microtubules [1,10], only three factors are essential for the dissipative assembly-disassembly cycles: (i) There is a pool of free ATP(GTP) resulting in a continuous supply of the ATP(GTP) species [1]; (ii) hydrolysis takes place at random subunits within the filaments [11,12]; and (iii) hydrolysis results in an increased dissociation rate [1]. A simple stochastic process incorporates these features and has been used before to model cytoskeletal filaments [11,13–21].

Here we introduce the general term *simple association dissociation aging process (SADAP)*, because there are diverse potential applications of this process. For instance, SADAPs may serve as stochastic models for (computer) stacks, also termed last in–first out (LIFO) queues, with two types of (data) packets: "Intact" packets enter the stack and leave it with a certain rate. While in the stack, these packets may become "corrupt" (no longer needed or damaged), leading to a larger stack leaving rate. Furthermore, a particular SADAP has been considered as a model for chaperone-assisted polymer translocation [22].

Three stochastic processes, all having exponentially distributed transition times, define the SADAP as a Markov process, see Fig. 1: (i) Subunits are incorporated with a constant rate ω_+ into the filament at one terminus called the *active end*. Upon incorporation, a subunit is in *state 1*. (ii) By means of *aging* with rate ω_a, any state-1 subunit within the filament can attain *state 0*. (iii) The subunit at the active end dissociates with rate $\omega_{-,1} \equiv \omega_1$ if it dwells in state 1 and with rate $\omega_{-,0} \equiv \omega_0$ if it dwells in state 0.

A crucial objective of statistical mechanics is the computation of the properties of a macroscopic system based on microscopic laws. For a SADAP, one aims to predict the (macroscopic) average filament growth or shrinkage from the (microscopic) association, dissociation, and aging rates (ω_+, ω_1, ω_0, ω_a). No standard techniques exist to determine the stationary weights of the microstates for such driven systems far from equilibrium [23,24], but exact results are known for particular one-dimensional systems [25]. To our knowledge, similar results have not been found for the SADAP and the most detailed studies have been published in the context of actin and microtubule assembly [11,13–20]. A mean-field solution was already obtained in 1986 [13], but it turns out that correlations are crucial. On these grounds previous

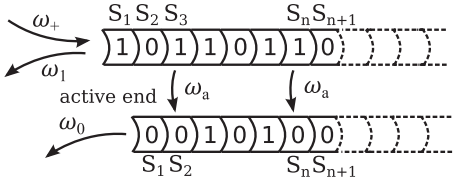

FIG. 1. Definition of simple association-dissociation-aging process (SADAP). The internal state of each subunit is described by a binary variable $S_i = 0,1$. State-1 subunits enter the filament at the active end with rate ω_+. State-1 subunits are converted into state-0 subunits by aging with rate ω_a. State-1 subunits (state-0 subunits) leave the filament at the active end with rate ω_1 (ω_0). The state of the N terminal subunits is represented by the sequence $(S_1, S_2, \ldots, S_N)$.

*thomas.niedermayer@mpikg.mpg.de

studies (including the very recent [20] which claims to account for correlations) lead to incorrect predictions of collective properties.

In this article, we present an analytical approach for solving the SADAP. We introduce an alternative form of the full master equation which describes all 2^N joint probabilities of the N terminal states. We found an ansatz for the steady-state solution which allowed us to derive a simple nonlinear recursion relation for all joint probabilities. This method enables the calculation of the filament growth and shrinkage velocities from the microscopic model parameters and the precise construction of the phase diagram. We found that our results are in excellent agreement with stochastic simulations.

The main sections (Secs. II–VIII) of the article provide a self-contained description of our ideas, procedure, and results, while Appendices A–F contribute details of the calculations and additional information.

II. GENERAL CONSIDERATIONS

In the limit of large times, a SADAP attains a nonequilibrium steady state: State 1 is supplied at the active end and used up by aging within the filament, whereas state 0 is supplied within the filament by aging and used up at the active end by dissociation. Therefore, the probability to find state 1 decreases monotonically with increasing distance from the active end, giving rise to a system which is not translationally invariant.

The filament growth velocity is determined by S_1, i.e., the state of the subunit at the active end, since $\omega_0 \neq \omega_1$ in general. The average growth velocity is given by $v = \omega_+ - (\omega_1 - \omega_0)\langle S_1\rangle - \omega_0$, where the average value $\langle S_1\rangle$ is the probability to find state 1 at the active end. The calculation of $\langle S_1\rangle$ is highly nontrivial and the most important result of our paper.

For the trivial case $\omega_+ = 0$, state-1 subunits are not added to the filament, and the steady state $\langle S_n\rangle = 0$ is attained, leading to $v = -\omega_0$. Furthermore, the transient dynamics is also well understood for this case, see Refs. [11,26] for detailed analyses in the context of actin filaments.

III. FULL MASTER EQUATION

For $\omega_+ > 0$, every subunit n within the filament has a finite probability $\langle S_n\rangle$ to be in state 1. The master equation for these probabilities reads [13,18]:

$$\begin{aligned}\partial_t \langle S_n\rangle &= \omega_+ \langle S_{n-1} - S_n\rangle + \omega_1 \langle S_1(S_{n+1} - S_n)\rangle \\ &\quad + \omega_0 \langle (1 - S_1)(S_{n+1} - S_n)\rangle - \omega_a \langle S_n\rangle, \qquad (1)\end{aligned}$$

where $S_0 \equiv 1$. This master equation does not fully capture the stochastic filament dynamics, as we will see below. In fact, the terms $\langle S_1 S_{n(+1)}\rangle$ reflect the coupling of aging to dissociation. So far, the mean-field approximation $\langle S_1 S_n\rangle \approx \langle S_1\rangle\langle S_n\rangle$ (for $n > 1$) has been employed [13,18] for uncoupling, but this leads to incorrect predictions, see Figs. 2, 3 and 4.

In order to account for correlations correctly, we thus need to investigate the full master equation. For a segment consisting of N subunits, this equation includes any combination of

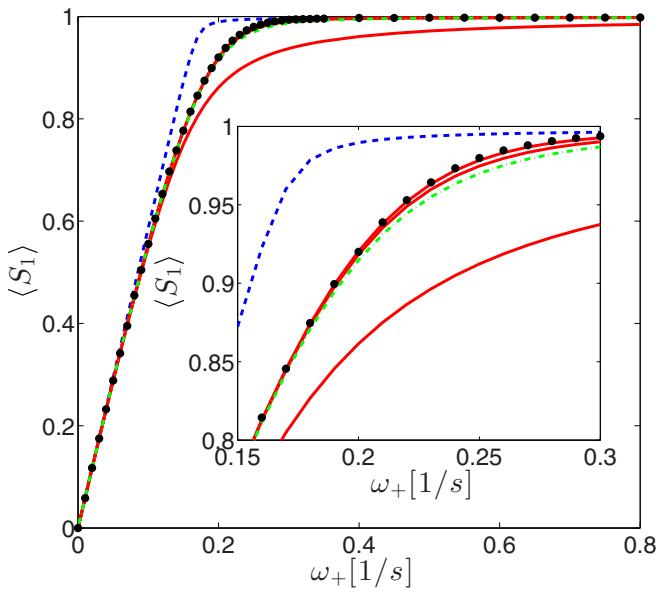

FIG. 2. (Color online) Probability $\langle S_1\rangle$ as a function of the association rate ω_+. Shown are analytical results employing the mean-field approximation [13] or the method in Ref. [20] (dashed blue line), the Eqs. (10) and (11) combined with the "mean-field cluster approximation" (cf. text, dash-dotted green line), and Eq. (12) with $g_1 = 0$, $g_3 = 0$, and $g_5 = 0$, respectively (three solid red lines). Simulation results are shown as black dots. Parameter values consistent with actin filaments are chosen, i.e., $\omega_1 = 0.16/\mathrm{s}$, $\omega_0 = 6/\mathrm{s}$, and $\omega_a = 0.01/\mathrm{s}$, see Ref. [11].

subunits $n_1, n_2, \ldots, n_m$, with $1 \leqslant n_1 < n_2 < \cdots < n_m \leqslant N$, i.e.,

$$\begin{aligned}&\partial_t \langle S_{n_1}\cdots S_{n_m}\rangle \\ &\quad = \omega_+ \langle S_{n_1-1}\cdots S_{n_m-1} - S_{n_1}\cdots S_{n_m}\rangle \\ &\qquad + \omega_1 \langle S_1 (S_{n_1+1}\cdots S_{n_m+1} - S_{n_1}\cdots S_{n_m})\rangle \\ &\qquad + \omega_0 \langle (1 - S_1)(S_{n_1+1}\cdots S_{n_m+1} - S_{n_1}\cdots S_{n_m})\rangle \\ &\qquad - \omega_a m \langle S_{n_1}\cdots S_{n_m}\rangle, \qquad (2)\end{aligned}$$

where, e.g., the ω_+ term accounts for gain $[\omega_+ \langle S_{n_1-1}\cdots S_{n_m-1}(1 - S_{n_1}\cdots S_{n_m})\rangle]$ and loss $[\omega_+ \langle S_{n_1}\cdots S_{n_m}(1 - S_{n_1-1}\cdots S_{n_m-1})\rangle]$ of probability by association of subunits. Since $S_0 \equiv 1$, Eq. (2) also holds for $n_1 = 1$. Both Eq. (1) and the master equations given in Ref. [20] are special cases of Eq. (2). Note that our requirement of increasing indices ensures $m \leqslant N$ and that the power set of $\{1,2,\ldots,N\}$ contains 2^N elements [27]. Therefore, by excluding the empty set, we have $2^N - 1$ variants of Eq. (2) which constitute a complete description of the 2^N states $(S_1,\ldots,S_N)$ of the terminal segment consisting of N subunits. Note that in the more common representation of these 2^N states by $P_{\alpha_1,\ldots,\alpha_N} \equiv \mathrm{prob}(S_1 = \alpha_1,\ldots,S_N = \alpha_N)$, one term is redundant, because of the normalization $\sum_{\alpha_1}\cdots\sum_{\alpha_N} P_{\alpha_1,\ldots,\alpha_N} = 1$. In this representation, the full

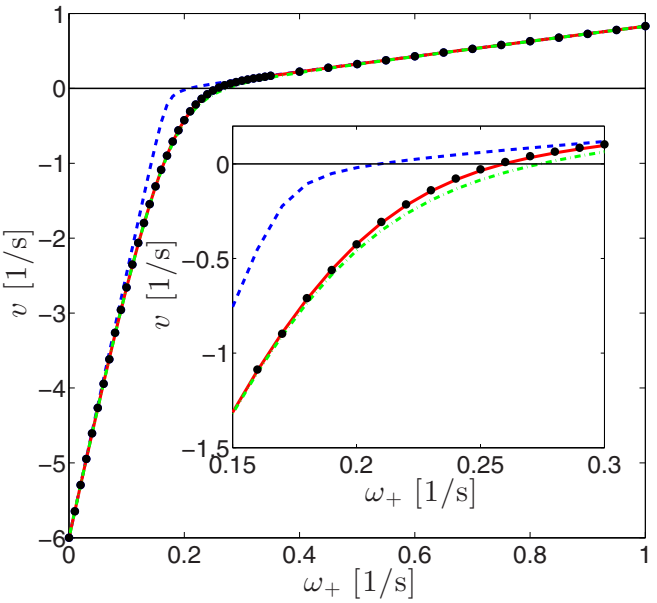

FIG. 3. (Color online) Average growth velocity v as a function of the association rate ω_+. The same parameter values and color code as in Fig. 2 are used. The solid red line corresponds to $g_5 = 0$.

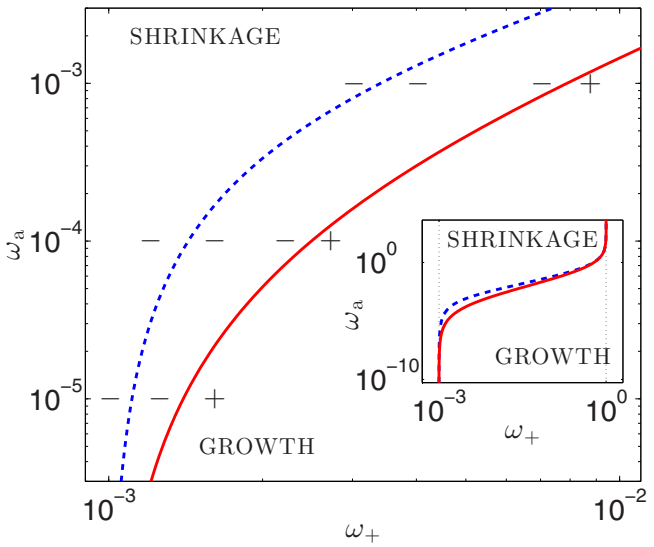

FIG. 4. (Color online) Phase diagram featuring growth and shrinkage phases. Shown is the (ω_+,ω_a) plane for the (rescaled) parameter values $\omega_0 = 1$ and $\omega_1 = 10^{-3}$. The (dashed) blue line represents the phase boundary ($v = 0$) as obtained from the mean-field approximation, while the (solid) red line was calculated via Eq. (12) with $g_5 = 0$. At the position of the + (–) signs, simulated filaments grow (shrink). This indicates that the red (solid) and not the blue (dashed) line represents the correct phase boundary. Inset: Complete phase diagram, where $v = 0$ is given by $\omega_+ = \omega_1$ for $\omega_a \to 0$, and $\omega_+ = \omega_0$ for $\omega_a \to \infty$.

master equation reads

$$\begin{aligned}\partial_t P_{\alpha_1,\ldots,\alpha_N} =& \omega_+\big(\alpha_1 P_{\alpha_2,\ldots,\alpha_N} - P_{\alpha_1,\ldots,\alpha_N}\big)\\ &+ \omega_1\big(P_{1,\alpha_1,\ldots,\alpha_N} - \alpha_1 P_{\alpha_1,\ldots,\alpha_N}\big)\\ &+ \omega_0\big(P_{0,\alpha_1,\ldots,\alpha_N} - (1-\alpha_1) P_{\alpha_1,\ldots,\alpha_N}\big)\\ &+ \omega_a \sum_{i=1}^{N}\big\{(1-\alpha_i) P_{\alpha_1,\ldots,1-\alpha_i,\ldots,\alpha_N}\\ &- \alpha_i P_{\alpha_1,\ldots,\alpha_N}\big\},\end{aligned} \tag{3}$$

where $P_{\alpha_2,\ldots,\alpha_N} \equiv \text{prob}(S_1 = \alpha_2,\ldots,S_{N-1} = \alpha_N) \equiv P_{\alpha_2,\ldots,\alpha_N,1} + P_{\alpha_2,\ldots,\alpha_N,0}$ is to be interpreted as a marginal probability. For instance, the gain and loss terms due to association of subunits are given by $\omega_+(\alpha_1(P_{\alpha_2,\ldots,\alpha_N,1} + P_{\alpha_2,\ldots,\alpha_N,0}) - \prod_{i=1}^N \alpha_i P_{\alpha_1,\ldots,\alpha_N})$ and $\omega_+(1 - \prod_{i=1}^N \alpha_i) P_{\alpha_1,\ldots,\alpha_N}$, respectively. The probabilities in Eqs. (2) and (3) may be transformed into one another by

$$P_{\alpha_1,\ldots,\alpha_N} \equiv \left\langle \prod_{i=1}^{N} (1-S_i)^{1-\alpha_i} S_i^{\alpha_i} \right\rangle, \tag{4}$$

$$\langle S_{n_1}\cdots S_{n_m}\rangle \equiv \sum_{\alpha_1,\alpha_2,\ldots,\alpha_{n_m}} P_{\alpha_1,\alpha_2,\ldots,\alpha_{n_m}} \prod_{i=1}^{m} \alpha_{n_i}. \tag{5}$$

IV. ANSATZ FOR STEADY-STATE SOLUTION

The steady-state solution of the master Eq. (2) can be constructed by the following ansatz. Since state 1 is only supplied at the active end, the probability $\langle S_n\rangle$ of finding state 1 at position n decreases with the distance from this terminus, motivating the ansatz $\langle S_{n+1}\rangle/\langle S_n\rangle = b_1$, i.e., shifting the subunit n by one decreases the probability $\langle S_n\rangle$ by the factor $b_1 < 1$. In fact, this ansatz was implicitly used in Ref. [13] to solve the mean-field approximation of Eq. (1). We generalize this relation of constant ratios by

$$\frac{\langle \prod_{i=1}^{k} S_{n_i} \prod_{j=k+1}^{m} S_{n_j+1}\rangle}{\langle \prod_{i=1}^{m} S_{n_i}\rangle} \equiv b_{m-k}, \tag{6}$$

where $n_1 < \cdots < n_m$ and $0 \leqslant k < m$. Shifting each of the $m-k$ subunits with indices $n_{k+1},\ldots,n_m$ by one decreases the joint probability $\langle S_{n_1}\cdots S_{n_k}\cdots S_{n_m}\rangle$ by the factor $b_{m-k} < 1$. By a successive use of this ansatz, see Appendix A for details, we find:

$$\left\langle \prod_{i=1}^{m} S_{n_i} \right\rangle = \prod_{i=0}^{m-1} b_{m-i}^{n_{i+1}-n_i-1}\, r_m, \tag{7}$$

where $r_m \equiv \langle S_1\cdots S_m\rangle$ and $n_0 \equiv 0$.

V. RECURSION RELATIONS

Next we derive conditional equations for the ratios b_m by inserting Eq. (7) into Eq. (2) at steady state and summing over all index combinations, i.e., $\sum_{n_1<\cdots<n_m}^{\infty} \partial_t \langle S_{n_1}\cdots S_{n_m}\rangle = 0$. We first consider the finite sum

$$\sum_{n_1=1}^{N} \sum_{n_2=n_1+1}^{n_1+N} \cdots \sum_{n_m=n_{m-1}+1}^{n_{m-1}+N} \partial_t \langle S_{n_1}\cdots S_{n_m}\rangle = 0 \tag{8}$$

and obtain the simple expression

$$\begin{aligned}&\omega_+\left(r_{m-1} - b_m^{N-1} r_m\right) + \omega_1\left(b_m^{N-1} r_{m+1} - r_m\right)\\ &+ \omega_0\left(b_m^N r_m - b_m^{N-1} r_{m+1}\right) - m\,\omega_a\, r_m \frac{1-b_m^N}{1-b_m} = 0,\end{aligned} \tag{9}$$

see Appendix B for details of the calculation. For $N \to \infty$, this equation leads to

$$b_m = \frac{\omega_+ r_{m-1} - (\omega_1 + m\,\omega_a)\, r_m}{\omega_+ r_{m-1} - \omega_1 r_m}, \tag{10}$$

for $m \geqslant 1$, where $r_0 \equiv 1$. Next we focus on the general case $\omega_0 \neq \omega_1$, while the trivial special case $\omega_0 = \omega_1$ is handled in Appendix C. For finite N, Eq. (9) leads to

$$r_{m+1} = \frac{\omega_+ r_{m-1} - (\omega_+ + \omega_1 + m\,\omega_a) r_m + \omega_0\, b_m\, r_m}{\omega_0 - \omega_1}, \tag{11}$$

for $m \geqslant 1$. Together with Eq. (7), the nonlinear recursion relations, Eqs. (10) and (11), allow us to express any $\langle S_{n_1} \cdots S_{n_m} \rangle$ and via Eq. (4) any $P_{\alpha_1,\ldots,\alpha_N}$ as an explicit function of r_1, i.e., the steady-state probability of the terminal subunit to attain state 1.

VI. CALCULATION OF r_1

For the steady-state solution of the full master equation (2), we need only one additional equation relating b_m and r_m, because we already have $2M$ Eqs. (10) and (11) for the $2M + 1$ unknowns $b_1, \ldots, b_M, r_1, \ldots, r_{M+1}$. Next we discuss four schemes (1)–(4) to obtain such an equation. While the options (1) and (2) reduce our approach to already-known mean-field results, (3) combines the recursions for b_m and r_m with the so-called "mean-field cluster approximation" [28] and yields considerably better results. Formidable results are obtained by scheme (4), which is also exact in a certain limit.

(1) The mean-field approximation $\langle S_1 S_n \rangle = \langle S_1 \rangle \langle S_n \rangle$ used in Refs. [13,18] could serve as a closure. This is equivalent to $r_2 = b_1 r_1^2$ which leads to a cubic Equation in r_1, see Appendix D 1. The solution from Refs. [13,18] is retrieved and shown in Fig. 2.

(2) Even though a correct treatment of correlations is claimed in Ref. [20], the mean-field approximation $\langle S_1 S_2 \rangle = \langle S_1 \rangle \langle S_2 \rangle$ is implicitly used in Eq. (18) of Ref. [20], as we show in Appendix D 2. In consequence, the method from Ref. [20] leads to the same closure relation and identical (mean-field) values for $\langle S_1 \rangle$.

(3) The "mean-field cluster approximation" [28] estimates the probability for a cluster of subunits from the probabilities of two subclusters. Combining this idea with our ansatz leads to more than one real solution with $0 \leqslant r_1 \leqslant 1$, see Appendix D 3 for details, from which we choose the particular r_1 with the closest distance to simulations, see Fig. 2.

(4) Some steady-state probabilities are negligibly small. Let us consider the 2^{N+1} states of the terminal segment consisting of $N + 1$ subunits. Since the probability to find state 1 decays with the distance from the terminus, the probability $P_{0,\ldots,0,1} \equiv \text{prob}(S_1 = 0, \ldots, S_N = 0, S_{N+1} = 1) \equiv g_N$ must be very small compared to other probabilities $P_{\alpha_1,\ldots,\alpha_N,\alpha_{N+1}}$ for all parameter values. Therefore, we obtain an approximation of order N by neglecting these states, i.e., setting $g_N = 0$. Note that this approximation differs fundamentally from truncating the system after a fixed number of subunits, see Fig. 5 for comparison. Next, we rewrite the probability g_N by expanding the product in Eq. (4), inserting

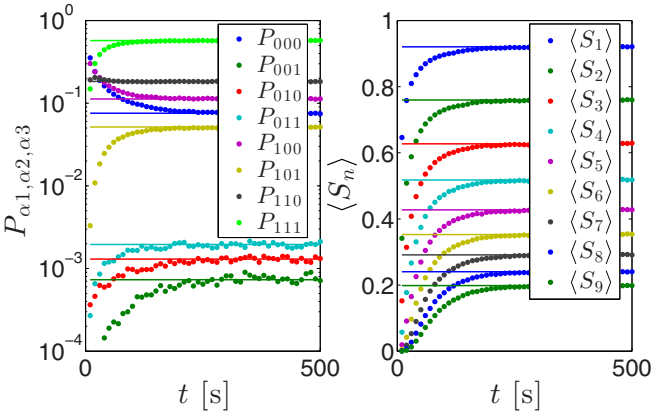

FIG. 5. (Color online) Joint probabilities $P_{\alpha_1,\alpha_2,\alpha_3} \equiv \text{prob}(S_1 = \alpha_1, S_2 = \alpha_2, S_3 = \alpha_3)$ and individual probabilities $\langle S_n \rangle$ as functions of time. The steady states from simulations (colored circles) of 10^5 filaments match the analytical results (colored lines) from Eq. (12) with $g_5 = P_{000001} = 0$. The joint probabilities $P_{\alpha_1,\alpha_2,\alpha_3}$ of particular configurations are very small, while $\langle S_n \rangle$ decays only with $\langle S_n \rangle = b_1^{n-1} r_1$, where $r_1 \simeq 0.920$ and $b_1 \simeq 0.826$. Parameter values as in Fig. 2 and with $\omega_+ = 0.2/\text{s}$.

Eq. (7) and rearranging the sum, see Appendix D 4 for details:

$$g_N = \sum_{m=0}^{N} (-1)^m\, r_{m+1} \sum_{k_1+\cdots+k_{m+1}=N-m} \prod_{i=1}^{m+1} b_{m+2-i}^{k_i}, \tag{12}$$

where we sum over all non-negative integers $k_1, \ldots, k_{m+1}$ for which $k_1 + \cdots + k_{m+1} = N - m$ holds. With Eqs. (10) and (11), g_N may be expressed as a rational function of r_1. For the first-order approximation, we have $g_1 = b_1^{(1)} r_1^{(1)} - r_2^{(1)} = 0$ which is equivalent to a quadratic equation in $r_1^{(1)}$ and has the unique solution $r_1^{(1)-}$ in the physical regime $0 \leqslant r_1^{(1)-} \leqslant 1$, see Appendix D 4 for details. For higher-order approximations, i.e., $N \geqslant 2$, there are $2^{N+1} - N - 1$ (complex) solutions $r_1^{(N)}$ and in particular there is more than one solution with $0 \leqslant r_1^{(N)} \leqslant 1$. We determine these solutions numerically and recursively identify the physical $r_1^{(N+1)}$ as the one which is closest to $r_1^{(N)}$, starting from the uniquely determined $r_1^{(1)}$, see Fig. 6.

VII. RESULTS

To validate our results, we performed extensive stochastic simulations, employing the Gillespie algorithm [29]. As expected, $r_1^{(N)}$ converges to $\langle S_1 \rangle = r_1^{(\text{sim})}$ from these simulations, see Figs. 2, 7, and 8. Likewise, the simulated velocities match the analytical results, see Figs. 3, 9, and 10.

The mean-field methods (1) and (2) explicated in Sec. VI systematically overestimate $\langle S_1 \rangle$, and therefore v, because they neglect correlations: Since $\omega_1 < \omega_0$, the presence of state-1 subunits within the filament increases its stability, i.e., its tendency to grow and hence its tendency to attain state 1 at the terminus. In consequence, there is a positive correlation between S_1 and S_n, and in particular $\langle S_1 S_2 \rangle > \langle S_1 \rangle \langle S_2 \rangle \equiv \langle S_1 S_2 \rangle_{\text{m.f.}}$, which leads to $\langle S_1 \rangle < \langle S_1 \rangle_{\text{m.f.}}$, see Fig. 2.

Our approach allows for the precise calculation of all joint probabilities, see Eq. (4) and Fig. 5, and all correlations, see Appendix E for details. As expected, maximal correlation coefficients are attained at parameter values corresponding to intermediate values of $\langle S_1 \rangle$, where neither state 1 nor state 0 dominates the terminus, see Fig. 11. As the mean-field approach systematically overestimates $\langle S_1 \rangle$, it underestimates the critical association rates, where the growth velocity vanishes, see Figs. 3, 9, and 10.

The presence of actin depolymerization factors (ADFs)/cofilins *in vivo* increases ω_0 [30] and leads to a much larger ratio ω_0/ω_1. In consequence, correlations are even more important and the mean-field approximation entirely fails, see Figs. 8 and 10. Parameter values of microtubules *in vitro* [5,10] are discussed in Appendix F and Figs. 7 and 9.

As the average growth-shrinkage behavior is the most prominent macroscopic property of a SADAP, it is desirable to precisely calculate the boundary between the growth ($v > 0$) and shrinkage ($v < 0$) phase in parameter space. By rescaling time in units of ω_0 and fixing ω_1, this boundary is represented by the line in Fig. 4. For $\omega_a \to 0$, the terminus is in state 1 and therefore the line is given by $\omega_+ = \omega_1$. Analogously, it is given by $\omega_+ = \omega_0$ for $\omega_a \to \infty$. Finding the boundary in general relies on the accurate calculation of $\langle S_1 \rangle$. Therefore mean-field solutions fail while our approach yields precise results, see Fig. 4.

VIII. CONCLUSION AND OUTLOOK

We have analytically investigated the simple association-dissociation-aging process (SADAP) and found an approach which permits the recursive solution of the full master equation (2). Most importantly, this enables the calculation of $\langle S_1 \rangle$ beyond mean field, see Fig. 2. We have precisely determined the average growth velocity v (Figs. 3, 9, and 10) and the phase diagram (Fig. 4). Furthermore, our approach allows for the calculation of the probabilities $P_{\alpha_1,\ldots,\alpha_N}$ (Fig. 5), correlation coefficients (Figs. 11 and 12), and the exact length distribution $\Pi_L \equiv r_L - r_{L+1}$ of the cap of state-1 subunits (Fig. 13). Via Eq. (7), we may also compute all higher-order correlation functions.

In vitro, cytoskeletal filaments often generate force by growing against an obstacle such as a cell membrane [5]. In that case, thermodynamics requires the association and/or dissociation rates to be force dependent. In the light of our results, the force-velocity relation has to be revalidated beyond the mean-field approximation. This can be readily performed with the presented approach.

Our calculations may also be generalized to more involved association-dissociation-aging processes in which, e.g., subunit aging depends on the states of neighboring subunits. The latter case has been discussed (but not solved) as "cooperative hydrolysis" for actin filaments [31] and microtubules [32].

In a similar way, as the totally asymmetric simple exclusion process is regarded a paradigm for one-dimensional transport [24,33–35], the SADAP may become a paradigmatic model for one-dimensional association-dissociation phenomena and our approach may help to understand nonequilibrium systems in general.

APPENDIX A: TRANSFORMATION OF THE ANSATZ

Here we explicate that the ansatz of constant ratios [Eq. (6)] is equivalent to Eq. (7). First, the m subunits in $\langle S_{n_1} \ldots S_{n_m} \rangle$ are simultaneously moved to the terminus. Applying Eq. (6) $n_1 - 1$ times with $k = 0$ results in

$$\left\langle \prod_{i=1}^{m} S_{n_i} \right\rangle = b_m^{n_1-1} \left\langle S_1 \prod_{i=2}^{m} S_{n_i-n_1+1} \right\rangle. \tag{A1}$$

Second, the subunits with indices $n_2 - n_1 + 1, \ldots, n_m - n_1 + 1$ are simultaneously moved and the ansatz is applied $n_2 - n_1 - 1$ times with $k = 1$:

$$\left\langle S_1 \prod_{i=2}^{m} S_{n_i-n_1+1} \right\rangle = b_{m-1}^{n_2-n_1-1} \left\langle S_1 S_2 \prod_{i=3}^{m} S_{n_i-n_2+2} \right\rangle. \tag{A2}$$

This procedure is repeated m times with $k = 0$, $k = 1$, $k = 2$, $\ldots$, $k = m - 1$. In the last step, the ansatz is employed $n_m - n_{m-1} - 1$ times with $k = m - 1$:

$$\left\langle \prod_{i=1}^{m-1} S_i \, S_{m-1+n_m-n_{m-1}} \right\rangle = b_1^{n_m-n_{m-1}-1} \left\langle \prod_{i=1}^{m} S_{n_i} \right\rangle. \tag{A3}$$

Combining these procedures leads to Eq. (7). On the other hand, Eq. (6) follows from Eq. (7) by insertion, establishing their equivalence.

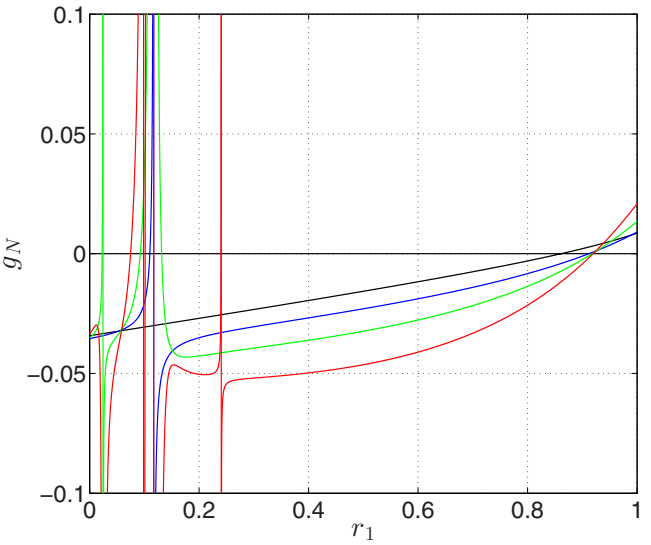

FIG. 6. (Color online) Expressions of g_N given by Eq. (12) as an explicit function of $r_1 \equiv \langle S_1 \rangle$. Shown are g_1 in black, g_2 in blue, g_3 in green, and g_4 in red. The first-order approximation $g_1 = 0$ provides a unique physical solution $0 \leqslant r_1^{(1)-} \leqslant 1$, see Eq. (D9), whereas higher-order approximations $g_N = 0$ exhibit more than one solution with $0 \leqslant r_1^{(N)} \leqslant 1$. As the physical solution of order $N + 1$ must resemble the physical solution of order N, the physical $r_1^{(N+1)}$ is uniquely determined as the one with the minimal distance to the physical $r_1^{(N)}$. For this graph, we have chosen parameter values which are consistent with actin filaments, i.e., $\omega_+ = 0.2/\mathrm{s}$, $\omega_1 = 0.16/\mathrm{s}$, $\omega_0 = 6/\mathrm{s}$, $\omega_a = 0.01/\mathrm{s}$, see Appendix F and Ref. [11]. We found $r_1^{(1)} \simeq 0.861$, $r_1^{(2)} \simeq 0.912$, $r_1^{(3)} \simeq 0.918$, and $r_1^{(4)} \simeq 0.920$, while stochastic simulations led to $\langle S_1 \rangle = r_1^{(\mathrm{sim})} \simeq 0.920$ and the mean-field approximation results in $r_1^{(\mathrm{mf})} \simeq 0.990$, cf. Fig. 2.

APPENDIX B: PERFORMING THE SUM IN EQ. (8)

We proceed by inserting Eq. (2) into Eq. (8) while employing the transformed ansatz [Eq. (7)]. For clarity, we first consider the auxiliary sums Σ_{I}, Σ_{II}, Σ_{III}, Σ_{IV}, and Σ_{V}.

$$\begin{aligned}\Sigma_{\mathrm{I}} &\equiv \sum_{n_1=1}^{N}\sum_{n_2=n_1+1}^{n_1+N}\cdots\sum_{n_m=n_{m-1}+1}^{n_{m-1}+N}\langle S_{n_1}\cdots S_{n_m}\rangle = r_m\sum_{n_1=1}^{N} b_m^{n_1-1}\sum_{n_2=n_1+1}^{n_1+N} b_{m-1}^{n_2-n_1-1}\cdots\sum_{n_m=n_{m-1}+1}^{n_{m-1}+N} b_1^{n_m-n_{m-1}-1}\\ &= r_m\sum_{n_1=0}^{N-1} b_m^{n_1}\sum_{n_2=0}^{N-1} b_{m-1}^{n_2}\sum_{n_3=0}^{N-1} b_{m-2}^{n_3}\cdots\sum_{n_m=0}^{N-1} b_1^{n_m} = r_m\prod_{i=1}^{m}\left(\frac{1-b_i^N}{1-b_i}\right), \qquad \text{(B1)}\end{aligned}$$

$$\begin{aligned}\Sigma_{\mathrm{II}} &\equiv \sum_{n_1=1}^{N}\sum_{n_2=n_1+1}^{n_1+N}\cdots\sum_{n_m=n_{m-1}+1}^{n_{m-1}+N}\langle S_{n_1-1}\cdots S_{n_m-1}\rangle\\ &= \sum_{n_2=2}^{N+1}\cdots\sum_{n_m=n_{m-1}+1}^{n_{m-1}+N}\langle S_0\, S_{n_2-1}\cdots S_{n_m-1}\rangle + \sum_{n_1=2}^{N}\sum_{n_2=n_1+1}^{n_1+N}\cdots\sum_{n_m=n_{m-1}+1}^{n_{m-1}+N}\langle S_{n_1-1}\cdots S_{n_m-1}\rangle\\ &= r_{m-1}\sum_{n_2=0}^{N-1}\cdots\sum_{n_m=0}^{N-1} b_{m-1}^{n_2}\cdots b_1^{n_m} + r_m\sum_{n_1=0}^{N-2}\sum_{n_2=0}^{N-1}\cdots\sum_{n_m=0}^{N-1} b_m^{n_1} b_{m-1}^{n_2}\cdots b_1^{n_m}\\ &= \left(r_{m-1}+\frac{1-b_m^{N-1}}{1-b_m}\,r_m\right)\prod_{i=1}^{m-1}\left(\frac{1-b_i^N}{1-b_i}\right), \qquad \text{(B2)}\end{aligned}$$

$$\Sigma_{\mathrm{III}} \equiv \sum_{n_1=1}^{N}\sum_{n_2=n_1+1}^{n_1+N}\cdots\sum_{n_m=n_{m-1}+1}^{n_{m-1}+N}\langle S_{n_1+1}\cdots S_{n_m+1}\rangle = b_m\Sigma_{\mathrm{I}}, \qquad \text{(B3)}$$

$$\begin{aligned}\Sigma_{\mathrm{IV}} &\equiv \sum_{n_1=1}^{N}\cdots\sum_{n_m=n_{m-1}+1}^{n_{m-1}+N}\langle S_1 S_{n_1}\cdots S_{n_m}\rangle\\ &= \sum_{n_2=2}^{N+1}\cdots\sum_{n_m=n_{m-1}+1}^{n_{m-1}+N}\langle S_1 S_{n_2}\cdots S_{n_m}\rangle + \sum_{n_1=2}^{N}\sum_{n_2=n_1+1}^{n_1+N}\cdots\sum_{n_m=n_{m-1}+1}^{n_{m-1}+N}\langle S_1 S_{n_1}\cdots S_{n_m}\rangle\\ &= \left(r_m+\frac{1-b_m^{N-1}}{1-b_m}\,r_{m+1}\right)\prod_{i=1}^{m-1}\left(\frac{1-b_i^N}{1-b_i}\right), \qquad \text{(B4)}\end{aligned}$$

and

$$\Sigma_{\mathrm{V}} \equiv \sum_{n_1=1}^{N}\cdots\sum_{n_m=n_{m-1}+1}^{n_{m-1}+N}\langle S_1 S_{n_1+1}\cdots S_{n_m+1}\rangle = r_{m+1}\prod_{i=1}^{m}\left(\frac{1-b_i^N}{1-b_i}\right). \qquad \text{(B5)}$$

Using the master Eq. (2), the terms with coefficients ω_+, ω_1, ω_0, and ω_{a} in the sum [Eq. (8)] are given by

$$\omega_+\left(\Sigma_{\mathrm{II}}-\Sigma_{\mathrm{I}}\right) = \omega_+\left(r_{m-1}-b_m^{N-1}\,r_m\right)\prod_{i=1}^{m-1}\left(\frac{1-b_i^N}{1-b_i}\right), \qquad \text{(B6)}$$

$$\omega_1\left(\Sigma_{\mathrm{V}}-\Sigma_{\mathrm{IV}}\right) = \omega_1\left(b_m^{N-1}\,r_{m+1}-r_m\right)\prod_{i=1}^{m-1}\left(\frac{1-b_i^N}{1-b_i}\right), \qquad \text{(B7)}$$

$$\omega_0\left[\Sigma_{\mathrm{III}}-\Sigma_{\mathrm{I}}-\left(\Sigma_{\mathrm{V}}-\Sigma_{\mathrm{IV}}\right)\right] = \omega_0\left(b_m^N\,r_m-b_m^{N-1}\,r_{m+1}\right)\prod_{i=1}^{m-1}\left(\frac{1-b_i^N}{1-b_i}\right), \qquad \text{(B8)}$$

$$\omega_{\mathrm{a}}\,m\,\Sigma_{\mathrm{I}} = \omega_{\mathrm{a}}\,m\,r_m\prod_{i=1}^{m}\left(\frac{1-b_i^N}{1-b_i}\right). \qquad \text{(B9)}$$

Now, plugging Eqs. (B6), (B7), (B8), and (B9) into Eq. (8) and dividing by $\prod_{i=1}^{m-1}\left(\frac{1-b_i^N}{1-b_i}\right)$ results in Eq. (9).

APPENDIX C: SPECIAL CASE $\omega_0 = \omega_1$

For this trivial special case, we find

$$\omega_+ r_{m-1} - (\omega_+ + \omega_1 + m\,\omega_a)\, r_m + \omega_1\, b_m\, r_m = 0 \qquad \text{(C1)}$$

instead of Eq. (11). Employing the case $m = 1$ of Eqs. (10) and (C1), we obtain a quadratic equation for r_1 which is solved by

$$r_1^{\pm} = \frac{\omega_+ + \omega_1 + \omega_a}{2\,\omega_1} \pm \sqrt{\frac{(\omega_+ + \omega_1 + \omega_a)^2}{4\,\omega_1^2} - \frac{\omega_+}{\omega_1}}. \qquad \text{(C2)}$$

This equation was found earlier [16,20].

APPENDIX D: DETAILS OF THE CALCULATION OF $r_1 \equiv \langle S_1 \rangle$

1. Mean field

With our ansatz, the mean-field approximation $\langle S_1 S_n \rangle = \langle S_1 \rangle \langle S_n \rangle$ translates into $r_2 = b_1\, r_1^2$. In fact, solving Eq. (1) of the main text for the mean-field case [13,18] requires the ansatz $\langle S_{n+1} \rangle / \langle S_n \rangle = b_1$, which is a special case of Eq. (6) for $m = 1$ and $k = 0$. Summing up Eq. (1) of the main text leads to

$$0 = \sum_{n=1}^{N} \partial_t \langle S_n \rangle = \omega_+ (1 - \langle S_N \rangle) + \omega_1 (\langle S_1 S_{N+1} \rangle - \langle S_1 \rangle)$$
$$+ \omega_0 (\langle S_{N+1} \rangle - \langle S_1 S_{N+1} \rangle) - \omega_a \sum_{n=1}^{N} \langle S_n \rangle. \qquad \text{(D1)}$$

For $N \to \infty$, we obtain

$$0 = \omega_+ - \omega_1 \langle S_1 \rangle - \omega_a \sum_{n=1}^{\infty} \langle S_n \rangle = \omega_+ - \omega_1 r_1 - \omega_a \frac{1}{1 - b_1}$$
$$\Leftrightarrow \; b_1 = \frac{\omega_+ - (\omega_1 + \omega_a) r_1}{\omega_+ - \omega_1\, r_1}, \qquad \text{(D2)}$$

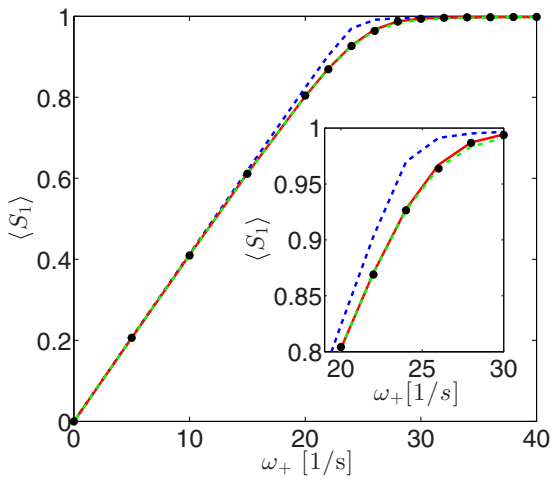

FIG. 7. (Color online) Probability $\langle S_1 \rangle$ as function of the association rate ω_+ for parameter values consistent with microtubules, i.e., $\omega_1 = 24/\text{s}$, $\omega_0 = 290/\text{s}$, and $\omega_a = 0.2/\text{s}$. The mean-field approximation [13] is shown as blue (dashed) line, the Eqs. (10) and (11) combined with the "mean-field cluster approximation" as the green (dash-dotted) line, and Eq. (12) with $g_5 = 0$ is displayed as the red (solid) line. Simulation results are shown as black dots.

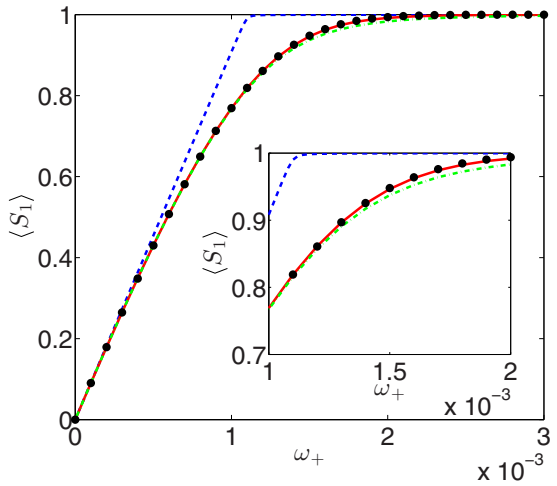

FIG. 8. (Color online) Probability $\langle S_1 \rangle$ as function of the association rate ω_+ for parameter values consistent with actin filaments in the presence of actin depolymerization factors (ADFs)/cofilins. The rates are rescaled to dimensionless form, see Appendix F for details, and given by $\omega_0 = 1$, $\omega_1 = 10^{-3}$, and $\omega_a = 10^{-4}$, respectively. The same color code as in Fig. 7 is used. Because $\omega_1/\omega_0 = 10^3 \gg 1$, correlations are very significant and the mean-field approach totally fails.

while for $N = 1$, we find

$$0 = \omega_+ - (\omega_+ + \omega_1 + \omega_a) r_1 + \omega_0 b_1 r_1 + (\omega_1 - \omega_0) r_2. \qquad \text{(D3)}$$

With the mean-field approximation $r_2 = b_1\, r_1^2$, these two equations lead to a cubic equation for r_1 which has one solution $0 \leqslant r_1 \leqslant 1$, cf. Ref. [18].

2. Approximation in Ref. [20]

A supposedly alternative approach was reported by Li *et al.* [20]. In fact, the approximation $\langle S_1 S_n \cdots S_{n+l-1} \rangle = \langle S_1 \rangle \langle S_n \cdots S_{n+l-1} \rangle$ is implicitly adopted in Eq. (18) of Ref. [20] for the case $\omega_0 \neq \omega_1$. This approximation and the ansatz in Eq. (4) of Ref. [20] allows for a complete solution of the

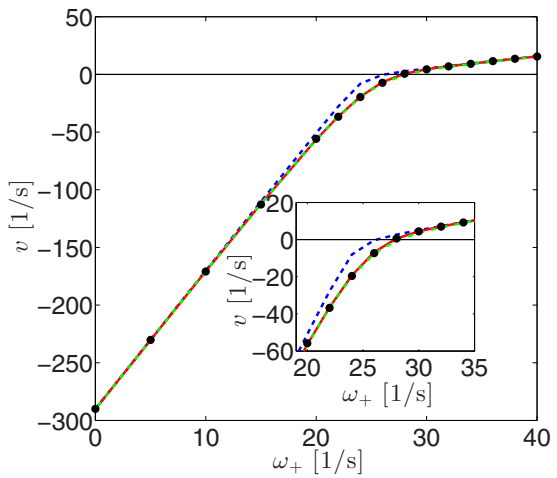

FIG. 9. (Color online) Average growth-shrinkage velocity v as functions of the association rate ω_+ for parameter values identical to Fig. 7 and consistent with microtubules. Same color code as in Fig. 7.

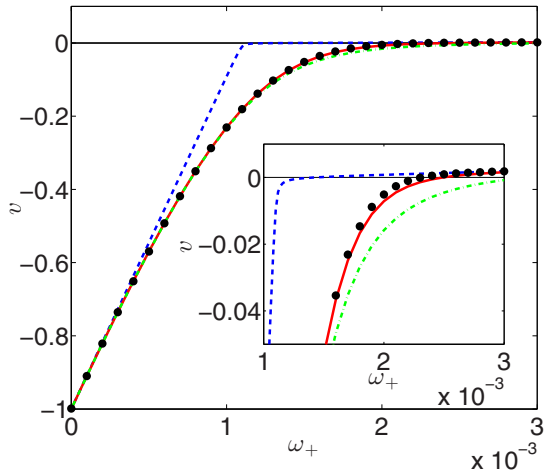

FIG. 10. (Color online) Average growth-shrinkage velocity v as functions of the association rate ω_+ for dimensionless parameter values identical to Fig. 8 and consistent with actin filaments in the presence of actin depolymerization factors (ADFs)/cofilins. Same color code as in Fig. 7. Because $\omega_1/\omega_0 = 10^3 \gg 1$, correlations are very significant and the mean-field approach totally fails.

SADAP. However, this solution is identical to the simple mean-field solution as can be seen from the special case $l = 1, n = 2$ (in the notation of Ref. [20]).

3. Cluster approximation

Another alternative is the "mean-field cluster approximation" [28] which estimates the probability $\langle S_1 S_2 S_3 \rangle$ by the probability $\langle S_1 S_2 \rangle$ times the conditional probability $\langle S_2 S_3 \rangle / \langle S_2 \rangle$. This leads to $r_3 \approx b_2 r_2^2/(b_1 r_1)$ and with the recursion Eqs. (10) and (11) to an equation of sixth order in r_1. A numerical analysis reveals that there is more than one real solution with $0 \leqslant r_1 \leqslant 1$. Therefore, we do not proceed with this approach but only choose the particular solution with the closest distance to the simulations, see Fig. 2.

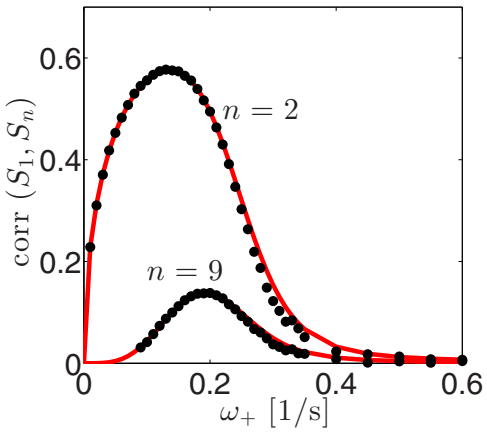

FIG. 11. (Color online) Dependence of correlation coefficient $\mathrm{corr}(S_1, S_n) \equiv \mathrm{cov}(S_1, S_n)/\sqrt{\mathrm{var}(S_1)\,\mathrm{var}(S_n)}$ on association rate ω_+ for $n = 2$ and $n = 9$. The black dots are obtained from simulations and the red lines are calculated from Eq. (E1) via Eq. (12) with $g_5 = 0$. Parameter values are consistent with actin filaments, i.e., $\omega_1 = 0.16/\mathrm{s}$, $\omega_0 = 6/\mathrm{s}$, and $\omega_a = 0.01/\mathrm{s}$ [11].

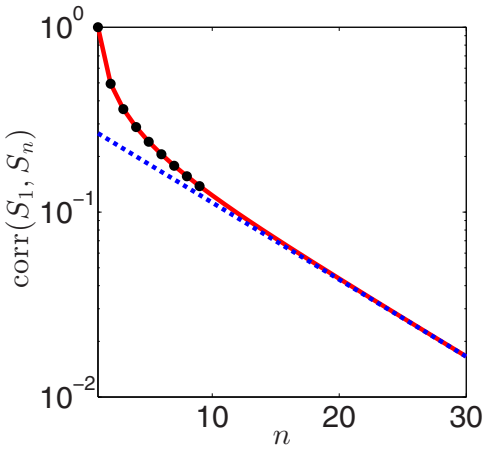

FIG. 12. (Color online) Decay of correlation coefficient for parameter values consistent with actin filaments, i.e., $\omega_1 = 0.16/\mathrm{s}$, $\omega_0 = 6/\mathrm{s}$, and $\omega_a = 0.01/\mathrm{s}$ [11] and association rate $\omega_+ = 0.2/\mathrm{s}$. The black dots are from simulations while the two lines are obtained via Eq. (12) with $g_5 = 0$. The red (solid) line is calculated from Eq. (E1) while the blue (dashed) line displays the asymptotic behavior, given by Eq. (E2).

4. Negligible probabilities

Equation (12) is derived as follows:

$$
\begin{aligned}
g_N &\equiv \left\langle \prod_{n=1}^{N} (1 - S_n)\, S_{N+1} \right\rangle \\
&= \left\langle \left[1 - \sum_{1 \leqslant n_1 \leqslant N} S_{n_1} + \sum_{1 \leqslant n_1 < n_2 \leqslant N} S_{n_1} S_{n_2} - \cdots \right.\right. \\
&\quad \left.\left. + (-1)^N\, S_1 \ldots S_N \right] S_{N+1} \right\rangle
\end{aligned}
\tag{D4}
$$

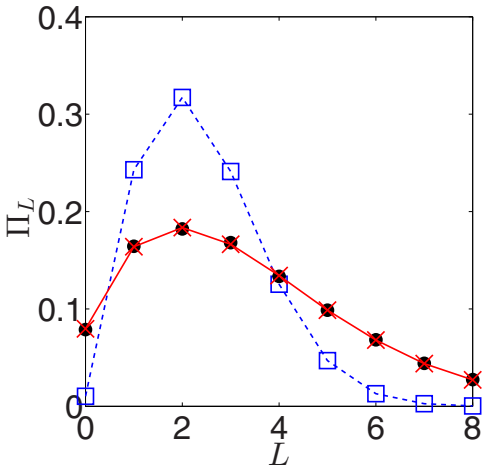

FIG. 13. (Color online) Distribution $\Pi_L \equiv r_L - r_{L+1}$ of the cap length L of state-1 subunits at the terminus, i.e., probability that the first L subunits are in state 1 while the subunit at position $L + 1$ attains state 0. The black dots are from simulations, while the blue squares are mean-field results and the red crosses are obtained via Eq. (12) with $g_5 = 0$. Apparently, correlations are significant for calculating the correct distribution. Parameter values as in Fig. 12.

$$= b_1^N\, r_1 + \sum_{m=1}^{N} (-1)^m \sum_{1\leqslant n_1<\cdots<n_m\leqslant N} b_{m+1}^{n_1-1}\, b_m^{n_2-n_1-1} \ldots \times b_2^{n_m-n_{m-1}-1}\, b_1^{N+1-n_m-1} \tag{D5}$$

$$= \sum_{m=0}^{N} (-1)^m\, r_{m+1} \sum_{k_1+\ldots k_{m+1}=N-m} \prod_{i=1}^{m+1} b_{m+2-i}^{k_i}\,, \tag{D6}$$

where we sum over all non-negative integers $k_1, \ldots, k_{m+1}$ for which $k_1 + \cdots + k_{m+1} = N - m$ holds. The expansion of the product in Eq. (D4) is performed in close analogy to the Mayer cluster expansion of an N-particle interaction gas [36]. In Eq. (D5), our ansatz is plugged in. Finally, the exponents were simplified by using $n_{i+1} \geqslant n_i + 1$, $N \geqslant n_m$ and the fact that all exponents sum up to $N - m$.

For the first-order approximation $g_1 = 0$, we have $r_2^{(1)} = b_1^{(1)}\, r_1^{(1)}$, where the superscript labels the order of approximation. Using the recursion relations in Eqs. (10) and (11), this leads to a quadratic equation for $r_1^{(1)}$ which is solved by

$$r_1^{(1)\pm} = \frac{\omega_+ + \omega_1 + \omega_a}{2\,\omega_1} \pm \sqrt{\frac{(\omega_+ + \omega_1 + \omega_a)^2}{4\,\omega_1^2} - \frac{\omega_+}{\omega_1}}. \tag{D7}$$

These solutions are identical to Eq. (C2), which is exact for the special case $\omega_0 = \omega_1$. Because of the inequality $\sqrt{\frac{(\omega_+ + \omega_1 + \omega_a)^2}{4\,\omega_1^2} - \frac{\omega_+}{\omega_1}} > \sqrt{\frac{(\omega_+ + \omega_1 + \omega_a)^2}{4\,\omega_1^2} - \frac{4\omega_1(\omega_+ + \omega_a)}{4\,\omega_1^2}}$, the solution $r_1^{(1)+}$ is unphysical, i.e.,

$$r_1^{(1)+} > \frac{\omega_+ + \omega_1 + \omega_a}{2\,\omega_1} + \frac{|\omega_+ + \omega_a - \omega_1|}{2\,\omega_1} \geqslant 1, \tag{D8}$$

while $r_1^{(1)-}$ is the unique physical solution since

$$0 \leqslant r_1^{(1)-} < \frac{\omega_+ + \omega_1 + \omega_a}{2\,\omega_1} - \frac{|\omega_+ + \omega_a - \omega_1|}{2\,\omega_1} \leqslant 1 \tag{D9}$$

holds.

APPENDIX E: CORRELATIONS

After having determined r_1 via Eq. (12), the recursion relations [Eqs. (10) and (11)] along with Eqs. (7) and (4) allow for the precise calculation of all joint probabilities $P_{\alpha_1,\ldots,\alpha_N}$ and all higher-order correlations $\mathrm{corr}(S_{n_1}, \ldots, S_{n_m})$. For instance, the (two-point) correlation coefficient of the first and the n-th state is given by

$$\mathrm{corr}(S_1, S_n) \equiv \frac{\mathrm{cov}(S_1, S_n)}{\sqrt{\mathrm{var}(S_1)\,\mathrm{var}(S_n)}} \equiv \frac{\langle S_1 S_n\rangle - \langle S_1\rangle\langle S_n\rangle}{\sqrt{\langle S_1\rangle\langle S_n\rangle(1-\langle S_1\rangle)(1-\langle S_n\rangle)}} = \frac{b_1^{n-2}\big(r_2 - b_1\, r_1^2\big)}{\sqrt{b_1^{n-1}\, r_1^2(1-r_1)\big(1-b_1^{n-1}\, r_1\big)}}, \tag{E1}$$

and its asymptotic behavior for large n reads

$$\mathrm{corr}(S_1, S_n) \sim_{n\to\infty} \frac{r_2 - b_1\, r_1^2}{b_1\, r_1 \sqrt{(1-r_1) b_1}}\; b_1^{n/2}, \tag{E2}$$

see Figs. 11 and 12.

APPENDIX F: DIFFERENT PARAMETER VALUES

The parameter values in Figs. 2, 3, and 5 are consistent with actin filaments: The random aging of subunits corresponds to the random release of inorganic phosphate, since the prior cleavage of bound ATP is more than an order of magnitude faster [37]. The dissociation of state-1 subunits correspond to the dissociation of ADP-Pi-actin from the barbed end, while the dissociation of state-0 subunits correspond to dissociation of ADP-actin from the barbed end. Therefore we have chosen $\omega_1 = 0.16/\mathrm{s}$, $\omega_0 = 6/\mathrm{s}$, and $\omega_a = 0.01/\mathrm{s}$, see Ref. [11]. The association rate ω_+ is variable and proportional to the concentration of ATP-actin monomers available for assembly.

For microtubules, the subunits represent tubulin dimers and the aging corresponds to hydrolysis of bound GTP which transforms GTP-tubulin into GDP-tubulin. This process occurs not only at the plus ends but also within microtubules [12], supporting our random aging model. Since there is controversy about the involved rates and exact mechanisms [10,38], we have simply chosen parameter values identical to Ref. [20], i.e., $\omega_1 = 24/\mathrm{s}$, $\omega_0 = 290/\mathrm{s}$, and $\omega_a = 0.2/\mathrm{s}$. Qualitatively, we find identical results to actin filaments, see Figs. 7 and 9.

The dynamics of actin filaments *in vivo* is affected by actin depolymerization factors (ADFs)/cofilins which selectively bind to ADP-actin subunits and increase the dissociation rate by a factor of 30 [30]. This leads to $\omega_0/\omega_1 \simeq 10^3$ and an increased importance of correlations. For the simulations, we have used dimensionless time and the rescaled rates $\omega_0 = 1$, $\omega_1 = 10^{-3}$, and $\omega_a = 10^{-4}$, see Figs. 4, 8, and 10.

[1] T. Pollard, W. Earnshaw, and J. Lippincott-Schwartz, *Cell Biology*, 2nd ed. (Saunders, Philadelphia, PA, 2007).

[2] F. Chiti and C. M. Dobson, Annu. Rev. Biochem. **75**, 333 (2006).

[3] T. Aida, E. Meijer, and S. Stupp, Science **335**, 813 (2012).

[4] D. Gross, J. F. Shortle, J. M. Thompson, and C. M. Harris, *Fundamentals of Queueing Theory*, 4th ed. (John Wiley & Sons, New York, 2013).

[5] J. Howard, *Mechanics of Motor Proteins and the Cytoskeleton* (Sinauer Associates, Sunderland, MA, 2001).

[6] T. Niedermayer, A. Jégou, L. Chièze, B. Guichard, E. Helfer, G. Romet-Lemonne, M. Carlier, and R. Lipowsky, Proc. Natl. Acad. Sci. USA **109**, 10769 (2012).

[7] T. Mitchison and M. Kirschner, Nature **312**, 237 (1984).

[8] K. A. Michie and J. Löwe, Annu. Rev. Biochem. **75**, 467 (2006).

[9] E. Korn, M.-F. Carlier, and D. Pantaloni, Science **238**, 638 (1987).

[10] A. Desai and T. J. Mitchison, Annu. Rev. Cell Dev. Biol. **13**, 83 (1997).

[11] A. Jégou, T. Niedermayer, J. Orbán, D. Didry, R. Lipowsky, M. Carlier, and G. Romet-Lemonne, PLoS Biol. **9**, e1001161 (2011).
[12] A. Dimitrov, M. Quesnoit, S. Moutel, I. Cantaloube, C. Poüs, and F. Perez, Science **322**, 1353 (2008).
[13] T. Keiser, A. Schiller, and A. Wegner, Biochemistry **25**, 4899 (1986).
[14] M. Bindschadler, E. Osborn, C. Dewey, Jr., and J. McGrath, Biophys. J. **86**, 2720 (2004).
[15] D. Vavylonis, Q. Yang, and B. O'Shaughnessy, Proc. Natl. Acad. Sci. USA **102**, 8543 (2005).
[16] E. Stukalin and A. Kolomeisky, Biophys. J. **90**, 2673 (2006).
[17] T. Antal, P. L. Krapivsky, S. Redner, M. Mailman, and B. Chakraborty, Phys. Rev. E **76**, 041907 (2007).
[18] P. Ranjith, K. Mallick, J.-F. Joanny, and D. Lacoste, Biophys. J. **98**, 1418 (2010).
[19] R. Padinhateeri, A. Kolomeisky, and D. Lacoste, Biophys. J. **102**, 1274 (2012).
[20] X. Li and A. B. Kolomeisky, J. Phys. Chem. B **118**, 2966 (2014).
[21] C. Erlenkämper and K. Kruse, J. Chem. Phys. **139**, 164907 (2013).
[22] P. Krapivsky and K. Mallick, J. Stat. Mech. Theor. Exp. (2010) P07007.
[23] B. Schmittmann and R. K. Zia, *Statistical Mechanics of Driven Diffusive Systems*, Vol. 17 (Academic Press, San Diego, CA, 1995).
[24] T. Chou, K. Mallick, and R. Zia, Rep. Prog. Phys. **74**, 116601 (2011).
[25] V. Privman, *Nonequilibrium Statistical Mechanics in One Dimension* (Cambridge University Press, Cambridge, 2005).
[26] T. Niedermayer, On the depolymerization of actin filaments, Ph.D. thesis, University of Potsdam, 2012.
[27] P. R. Halmos, *Naive Set Theory* (Springer, Berlin, 1960).
[28] D. ben-Avraham and J. Köhler, Phys. Rev. A **45**, 8358 (1992).
[29] D. T. Gillespie, J. Phys. Chem. **81**, 2340 (1977).
[30] M.-F. Carlier, F. Ressad, and D. Pantaloni, J. Biol. Chem. **274**, 33827 (1999).
[31] M.-F. Carlier, D. Pantaloni, and E. Korn, J. Biol. Chem. **262**, 3052 (1987).
[32] H. Flyvbjerg, T. E. Holy, and S. Leibler, Phys. Rev. Lett. **73**, 2372 (1994).
[33] J. Krug, Phys. Rev. Lett. **67**, 1882 (1991).
[34] B. Derrida, Phys. Rep. **301**, 65 (1998).
[35] M. Gorissen, A. Lazarescu, K. Mallick, and C. Vanderzande, Phys. Rev. Lett. **109**, 170601 (2012).
[36] R. P. Feynman, *Statistical Mechanics–A Set of Lectures*, 2nd ed. (Westview Press, Boulder, CO, 1998).
[37] M.-F. Carlier and D. Pantaloni, Biochemistry **25**, 7789 (1986).
[38] M. K. Gardner, B. D. Charlebois, I. M. Jánosi, J. Howard, A. J. Hunt, and D. J. Odde, Cell **146**, 582 (2011).